fire

MDPI

Technical Note

Investigation of the Temperature Beneath Curved Tunnel Ceilings Induced by Fires with Natural Ventilation

Haowen Tao *, Zhisheng Xu and Dongmei Zhou

School of Civil Engineering, Central South University (CSU), Changsha 410075, China; zhshxu@csu.edu.cn (Z.X.); 204811140@csu.edu.cn (D.Z.)
* Correspondence: hw.tao@csu.edu.cn; Tel.: +86-731-8265-5177

Abstract: The distribution characteristics of the temperature below ceilings in curved tunnel fires have not been quantitatively studied. A small-scale tunnel was constructed in this work to study the maximum temperature and longitudinal attenuation of the temperature below ceilings induced by fires in a curved tunnel with natural ventilation. Different tunnel turning radiuses and fire heat release rates were taken into account. The results show that the distribution characteristics of temperature below the tunnel ceiling is hardly affected by the tunnel turning radius in a scenario where the flame plume impinges on the ceiling (strong-plume-driven). The fire-induced maximum temperature and longitudinal attenuation of temperature in curved tunnels are comparable to those of straight tunnels. Improved correlations are proposed for the condition of a strong-plume-driven ceiling jet, and the measured value of the temperature of the experiment collapsed well. This work may enhance the understanding of temperature distributions in curved tunnel fires.

Keywords: curved tunnel fire; naturally ventilated tunnel; maximum temperature; longitudinal temperature attenuation

check for updates

Citation: Tao, H.; Xu, Z.; Zhou, D. Investigation of the Temperature Beneath Curved Tunnel Ceilings Induced by Fires with Natural Ventilation. *Fire* **2022**, *5*, 90. https://doi.org/10.3390/fire5040090

Academic Editors: Chuangang Fan and Dahai Qi

Received: 26 May 2022
Accepted: 22 June 2022
Published: 27 June 2022

1. Introduction

The construction of urban tunnels in metropolitan areas provides an effective solution for traffic congestion [1]. Curved tunnels are commonly used [2] as parts of urban tunnel systems (for example, large underground interconnected infrastructure, urban traffic link tunnels, etc.). Depending on the tunnel length, parts of the urban tunnels can be operated under natural ventilation. However, it appears that little research has been conducted on the temperatures below curved tunnel ceilings induced by fires under a natural ventilation scenario.

Maximum temperature rise and longitudinal temperature attenuation properties are two aspects of concern in a tunnel fire [3–5] and can serve as references for tunnel fire protection. In 1972, Alpert [6] presented a model for the prediction of maximum temperature rise induced by fires, given as:

$$\Delta T_m = 16.9\frac{\dot{Q}^{2/3}}{H_{ef}^{5/3}} \tag{1}$$

where ΔT_m is the maximum temperature rise below the ceiling (K), H_{ef} is the distance between the fire surface and the ceiling in the vertical direction (m), and $\dot{Q}$ is the fire heat release rate (kW).

In addition, in 1979 Heskestad and Delichatsios proposed the following equation for maximum temperature rise prediction in dimensionless form [7]:

$$\frac{\Delta T_m}{T_\infty} = 6.3\dot{Q}^{*2/3} \tag{2}$$

where $\dot{Q}^*$ can be calculated as:

$$\dot{Q}^* = \frac{\dot{Q}}{\rho_\infty T_\infty c_p \sqrt{g} H_{ef}^{5/2}}, \tag{3}$$

where T_∞, ρ_∞, and c_p are the temperature (K), density (kg/m^3), and specific heat at a constant pressure (kJ/(kg·K)) of ambient air, respectively, and g is the acceleration of gravity (m/s^2).

It should be noted that for a specified scenario where T_∞, ρ_∞, and c_p are constants expressions of Equations (1) and (2) will be similar.

As for the longitudinal temperature attenuation, Delichatsios [8] investigated the phenomenon of smoke spreading along a beamed ceiling in building fires, and proposed a correlation for the longitudinal temperature attenuation, given as:

$$\frac{\Delta T_x}{\Delta T_0}\left(\frac{l}{H}\right)^{1/3} = 0.49 e^{-6.67 St\left[\frac{x}{H}\cdot\left(\frac{l}{H}\right)^{1/3}\right]}, \tag{4}$$

where ΔT_x is the temperature rise for a certain position denoted x (K), l is the half width between the beams (m), x is the distance between the fire source and the position x in the horizontal direction (m), H is the height of the ceiling (m), and St represents the Stanton number.

It is noted that both the models of the maximum temperature and the temperature attenuation were originally used for building fires. It was then proven by other scholars that the predicted model for tunnel fires was similar. Li et al. [9] proposed a correlation for the maximum temperature in tunnel fires. For scenarios with natural ventilation, the correlation is similar to Equation (1), and is given as:

$$\Delta T_m = 17.5 \frac{\dot{Q}^{2/3}}{H_{ef}^{5/3}}. \tag{5}$$

Meanwhilem Hu et al. [10] indicated that the temperature attenuation along the tunnel can be expressed using an exponential function, which is given as:

$$\frac{\Delta T_x}{\Delta T_0} = e^{-Kx} \tag{6}$$

where ΔT_0 is the temperature rise at the point of reference (K), and K is a coefficient.

In addition, it has been shown in previous studies that the temperature in a tunnel fire can be affected by various aspects, such as the tunnel geometry, inclination, location of fires, ventilation conditions, vehicle blockage, etc. [11–16].

Zhang et al. [13] revealed that the maximum temperature below the tunnel ceiling varies with the tunnel slope. Their results showed that an increase in the tunnel slope decreases the maximum temperature. Based on these findings, a correlation of maximum temperature induced by fires for a sloping tunnel was proposed. Tang et al. [15] indicated that the maximum temperature below tunnel ceilings is influenced by the variation of fire locations in the transverse direction through experimental studies. A dimensionless coefficient k was introduced to modify the effect of different fire-source locations. The effect of mechanical smoke extraction was also discussed [16], in which the characteristic smoke attenuation in the transverse direction was presented. Ingason [17] conducted a small-scale fire test to reveal the tunnel fire behaviors under longitudinal ventilation. It was shown that the ventilation velocity has little effect on the maximum temperature for a fire source with a full-scale heat release rate larger than 100 MW. Chen [18] conducted a small-scale experiment to study the temperature attenuation in longitudinally ventilated tunnels, in which the modified characteristic length was introduced to develop a predictive correlation. Tao et al. [19] experimentally investigated the temperature profile induced by fires in a tunnel with the centralized smoke exhaust on a single side. The influence of vehicle blockage on maximum temperature under longitudinal ventilation was investigated by Tang et al. [20], in which different distances between the fire source and the blockage were taken into account.

However, the former models of temperature distribution beneath the ceilings of tunnel fires were established based on straight tunnels. When fire occurs in a curved tunnel, the resistance of smoke flow spreading differs from that in a straight tunnel [21]. The results of former studies show that the curve of a tunnel leads to a different characteristic of smoke spread under longitudinally forced ventilation [22,23]. However, the effect of tunnel turning radius on the spread of fire smoke and temperature distribution in a naturally ventilated tunnel has not been considered.

In this study, an investigation is conducted via a small-scale curved tunnel experiment to disclose the temperature profiles induced by fires (both maximum temperature rise and longitudinal temperature attenuation) below tunnel ceilings. Improved correlations are provided that may be helpful for understanding smoke spreading characteristics in a curved tunnel.

2. Experimental Setup

2.1. Small-Scale Curved Tunnel

A small-scale curved tunnel is constructed based on the Froude scaling law [24,25], whose dimensions are 3 m in length, 0.22 m in height, and 0.32 m in width. Figure 1 shows the apparatus of the small-scale curved tunnel. Fire-proof glass with a thickness of 6 mm is adopted for the tunnel sidewalls and a fire-proof plate with a thickness of 3 mm is used for the tunnel ceiling.

Figure 1. Apparatus of small-scale curved tunnel.

Figure 2 shows the thermocouple arrangement in the small-scale curved tunnel. The tunnel longitudinal length and tunnel turning radius are also shown in Figure 2. The longitudinal length of the tunnel is defined as the length of the tunnel centerline. Thermocouples of K type are used for temperature measuring, which are placed 0.01 m below the tunnel ceiling. The thermocouple intervals in the longitudinal direction are set to be 0.2 m. To accurately measure the maximum temperature, a smaller longitudinal interval of 0.066 m and 0.033 m is adopted near the fire source.

As shown in Figure 2, the tunnel section between the entrance and the fire source is defined as being upstream of the fire source. The tunnel section between the exit and the fire source is defined as being downstream of the fire source. The artificial fire source system consists of a propane cylinder, a fuel pipeline, a mass flow controller, and a steel burner. The outlet size of the steel burner is 0.03 m × 0.03 m. During the experiment, the fire source is placed on the centerline of the tunnel at a distance of 1.4 m from the tunnel entrance. High-purity propane is adopted to produce artificial fire, whose supply rate is monitored by a digital mass flow controller.

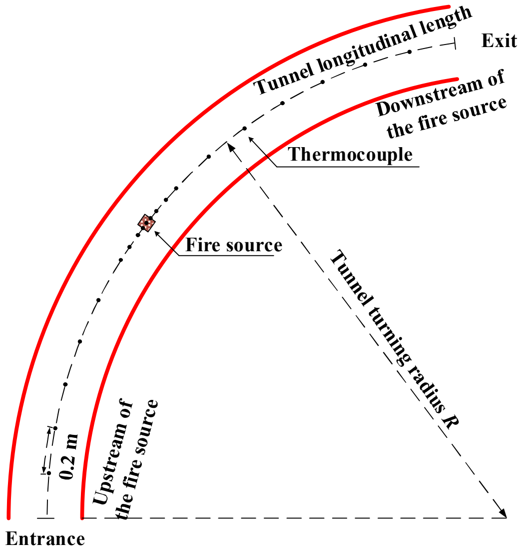

Figure 2. Thermocouple arrangement in a small-scale curved tunnel.

2.2. Experimental Scenarios

Table 1 summarizes the scenarios enacted in the small-scale experiments. A total of 28 scenarios were enacted, in which four different turning radiuses and seven different heat release rates are taken into account. The tunnel turning radius R = ∞ denotes a straight tunnel.

Table 1. The experimental scenarios conducted in the small-scale curved tunnel.

Scenarios No.	Fire Heat Release Rates (kW)	Tunnel Turning Radius R (m)
1–4	0.76	
5–8	1.01	
9–12	1.62	
13–16	2.03	3.5, 4.35, 8, ∞
17–20	2.43	
21–24	3.05	
25–28	4.06	

3. Results and Discussion

3.1. Variations in Maximum Temperature

Figure 3 depicts an instantaneous flame image observed in the experiment with different heat release rates. The phenomenon of flame plume impingement on the tunnel ceiling is observed even at smaller heat release rates. For instance, for $\dot{Q} = 0.76$ kW and 1.01 kW, the flame tip is close to the ceiling, and the thermocouple above the fire source is in direct contact with the flame.

Figure 4 plots the measured value of maximum temperature rise versus the turning radius, from which the influence of different turning radiuses can be recognized. The dotted lines represent the average temperature of different turning radiuses for the given heat release rate. It has been disclosed that the measured maximum temperature for different tunnel turning radiuses is nearly identical, which also indicates that the tunnel turning radius has little impact on the variation in maximum temperature.

(**a**) (**b**) (**c**) (**d**) (**e**)

Figure 3. Instantaneous flame image with different HRRs: (**a**) $\dot{Q}$ = 0.76 kW; (**b**) $\dot{Q}$ = 1.01 kW; (**c**) $\dot{Q}$ = 1.62 kW; (**d**) $\dot{Q}$ = 2.43 kW; (**e**) $\dot{Q}$ = 4.06 kW.

The phenomenon of fire plume impingement in the tunnel can be clearly observed for all scenarios in the experiment. The flame height is almost equivalent to the source-ceiling height, i.e., the ceiling jet is driven by a strong plume. The temperature directly above the fire source mainly relates to the temperature of the impinged plume, which is one of the reasons why the tunnel turning radius has little effect.

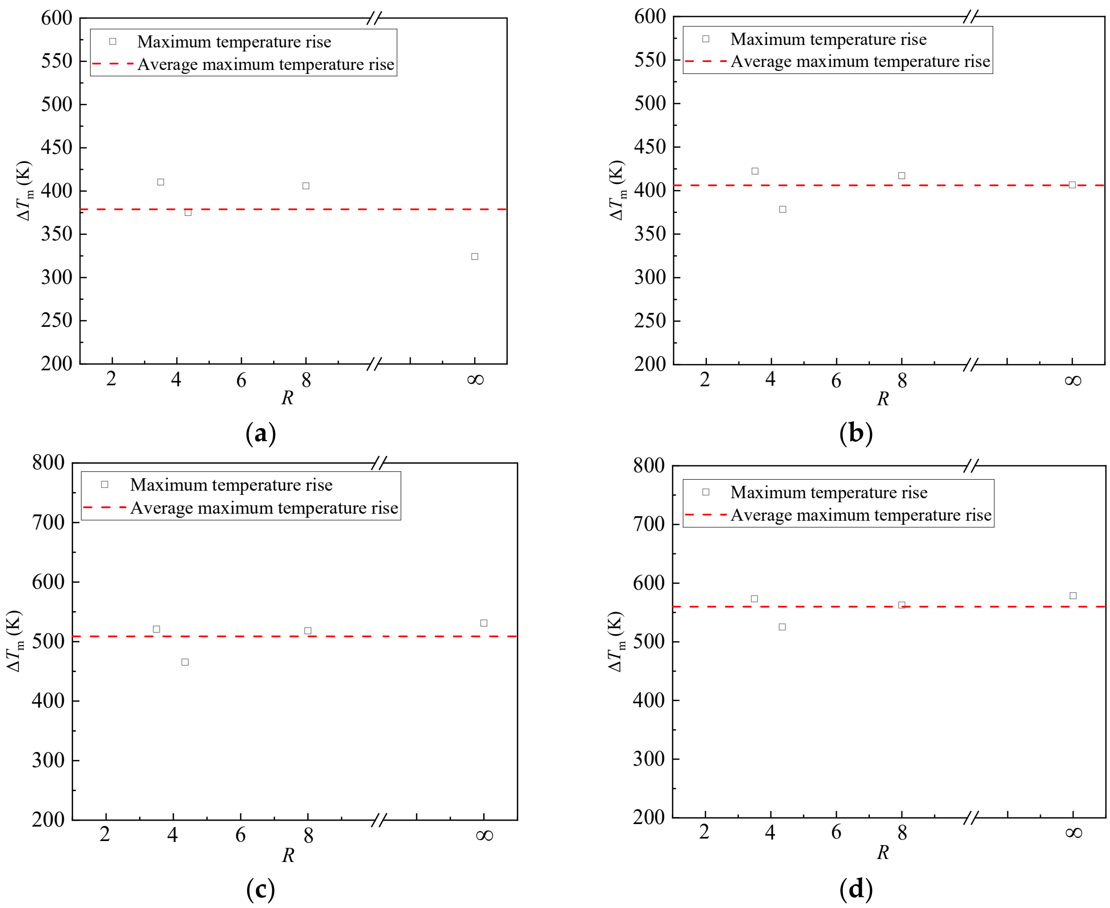

Figure 4. *Cont.*

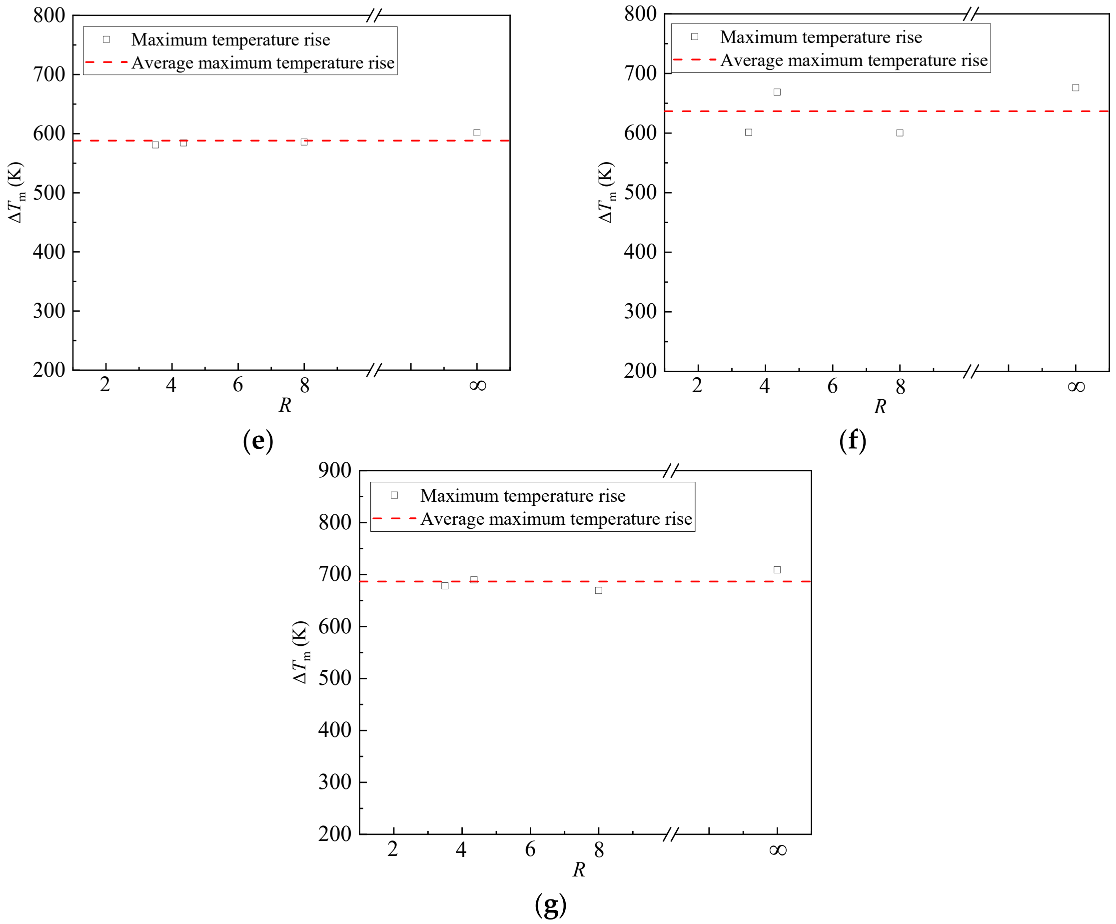

Figure 4. Measured value of maximum temperature rise (ΔT_m) against the tunnel turning radius: (**a**) $\dot{Q}$ = 0.76 kW; (**b**) $\dot{Q}$ = 1.01 kW; (**c**) $\dot{Q}$ = 1.62 kW; (**d**) $\dot{Q}$ = 2.03 kW; (**e**) $\dot{Q}$ = 2.43 kW; (**f**) $\dot{Q}$ = 3.05 kW; (**g**) $\dot{Q}$ = 4.06 kW.

The measured maximum temperature of all the experimental scenarios is compared with the predicted model proposed by Li et al. [9]. Figure 5 plots the measured value of maximum temperature as a function of $\dot{Q}^{2/3} H_{ef}^{5/3}$, along with Equation (5). It seems that the measured temperature in this work is significantly higher than the prediction based on Equation (5). This deviation is because Equation (5) is based on the theory of a "weak plume", whereas the ceiling jet condition in this work is more in accordance with the "strong plume driven" condition. As a result, the measured data cannot be accurately described by previously given correlation.

A predicted correlation of the temperature rise along the fire plume was proposed by McCaffrey and is given as [26]:

$$2g\frac{\Delta T}{T_\infty} = \left(\frac{\kappa}{C}\right)^2 \cdot \left(\frac{z}{\dot{Q}^{2/5}}\right)^{2\eta-1} \tag{7}$$

where z is the distance from the fire source in the vertical direction (m), ΔT is the temperature rise at the height of z (K), and κ, C, and η are constants whose values are shown in Table 2.

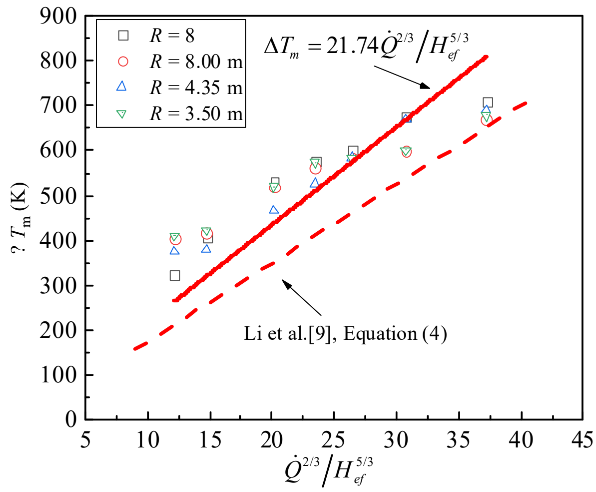

Figure 5. Prediction of maximum temperature rise (ΔT_m) based on Equation (5).

Table 2. Empirical constants in Equation (7).

Zone	κ	C	η
Continuous flame	6.9	0.9	1/2
Intermittent flame	1.9	0.9	0
Buoyant plume	1.1	0.9	−1/3

The fire plume temperature at the same height as the ceiling is given as:

$$\Delta T_m \propto \Delta T = \frac{T_\infty}{2g}\left(\frac{\kappa}{C}\right)^2 \cdot \left(\frac{z}{\dot{Q}^{2/5}}\right)^{2\eta-1}. \tag{8}$$

Equation (8) can be given in a dimensionless form as:

$$\frac{\Delta T_m}{T_\infty} \propto \left(\frac{H_{ef}/D_h}{\dot{Q}_s^{*2/5}}\right)^{\alpha}, \tag{9}$$

$$\dot{Q}_s^{*} = \frac{\dot{Q}}{\rho_\infty T_\infty c_p \sqrt{g} D_h^{5/2}}, \tag{10}$$

where: D_h is the hydraulic diameter of the burner outlet (m), α is constant, and $\dot{Q}_s^{*}$ is the heat release rate in dimensionless form using D_h as a characteristic length.

Figure 6 plots the measured maximum temperature rise versus the heat release rate in dimensionless form based on Equation (9), in which a good agreement between Equation (9) and experimental data is shown. The correlation in Figure 6 can be given as:

$$\frac{\Delta T_m}{T_\infty} = 4.79\left(\frac{H_{ef}/D_h}{\dot{Q}_s^{*2/5}}\right)^{-1} 1.8 \leq \frac{H_{ef}/D_h}{\dot{Q}_s^{*2/5}} \leq 3.7 \tag{11}$$

The tunnel ceiling dimensionless maximum temperature rise is related to −1 power of the distance between the fire surface and the ceiling in the vertical direction H_{ef}, indicating that the intermittent flame zone impinges on the ceiling, which is consistent with the phenomenon observed in our experiments.

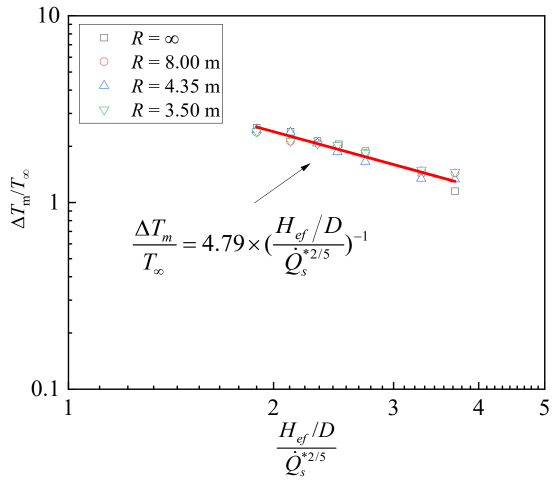

Figure 6. Predicted correlation of maximum temperature for the scenario of strong plume-driven ceiling jet.

3.2. The Longitudinal Attenuation of Temperature

The longitudinal attenuation of the temperature below ceilings is depicted in Figure 7 for a straight tunnel ($R = \infty$) with various heat release rates, where d denotes the longitudinal distance between the fire source and the temperature measuring point. For a given measuring position, the measured temperature rise (ΔT_d) increases with the heat release rate. As the distance from the fire source increases, the temperature decreases gradually. The temperature attenuation in both the upstream and downstream direction were found to be nearly identical. Therefore, only the temperature attenuation in the downstream direction is discussed.

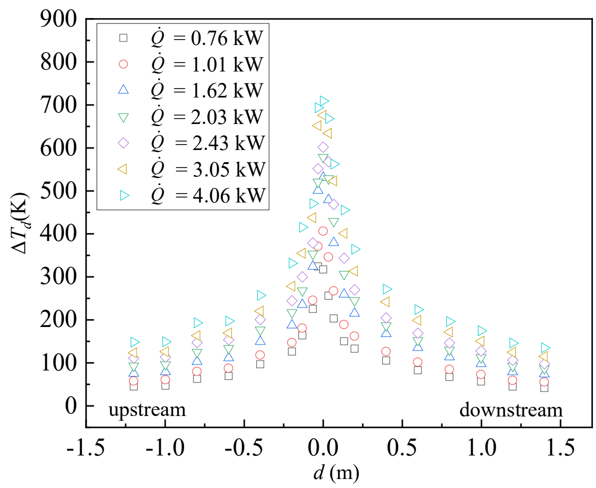

Figure 7. Longitudinal attenuation of the temperature of the longitudinal direction in a straight tunnel ($R = \infty$).

Figure 8 depicts the longitudinal attenuation of the temperature below ceilings with different turning radiuses. The temperature decay rate between a straight tunnel and a curved tunnel is similar for a given heat release rate, which indicates that the turning radius has little influence on smoke spread under natural ventilation.

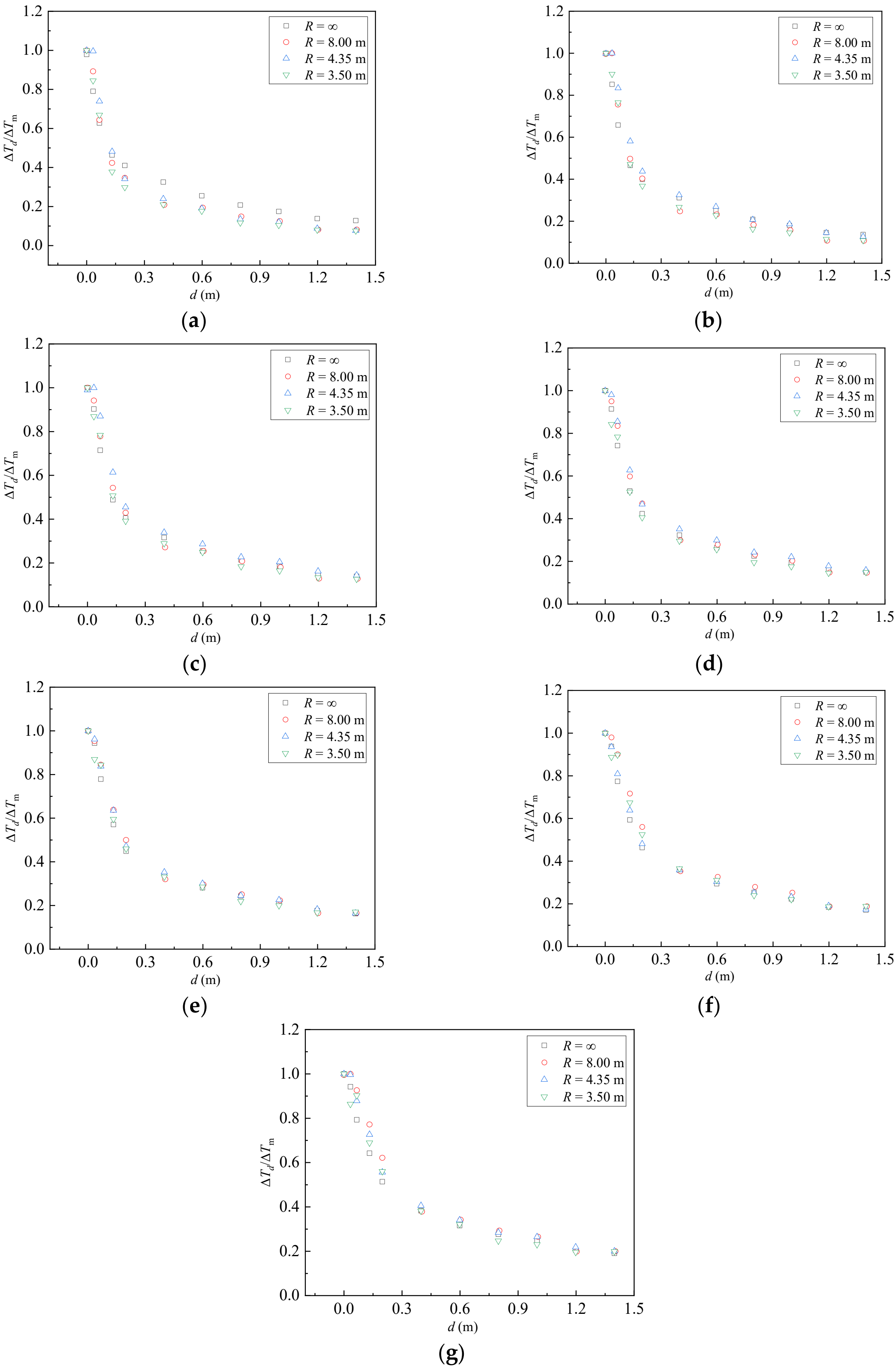

Figure 8. Longitudinal attenuation of temperature below the tunnel ceiling with different turning radiuses: (**a**) ΔT_m) against the tunnel turning radius: (**a**) $\dot{Q} = 0.76$ kW; (**b**) $\dot{Q} = 1.01$ kW; (**c**) $\dot{Q} = 1.62$ kW; (**d**) $\dot{Q} = 2.03$ kW; (**e**) $\dot{Q} = 2.43$ kW; (**f**) $\dot{Q} = 3.05$ kW; (**g**) $\dot{Q} = 4.06$ kW.

Figure 9 shows the temperature attenuation of all the experimental scenarios based on Equation (6). The scattering of the experimental data can be clearly observed. It may be suspected that the measurement points from which the maximum temperature is measured cannot serve as the reference point (ΔT_0) for the condition of strong plume impingement since it is not within the region of "one-dimensional flow".

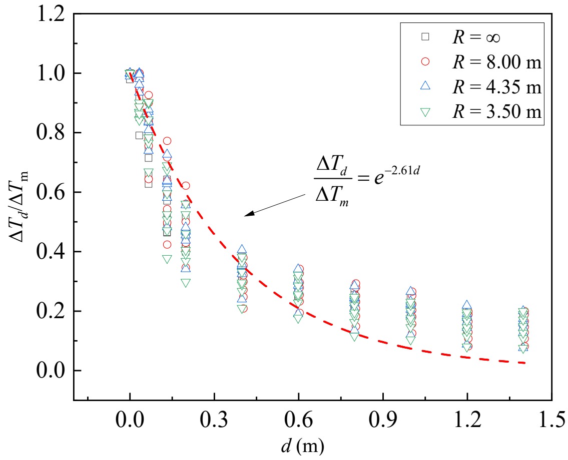

Figure 9. Plotting of temperature attenuation based on Equation (6).

To establish the relationship between the maximum temperature and longitudinal temperature attenuation, Heskestad and Hamada's [27] correlation is introduced, which was originally used for the temperature attenuation under an unconfined ceiling. It is given as:

$$\frac{\Delta T_r}{\Delta T_m} = 1.92\left(\frac{r}{b}\right)^{-1} - e^{[1.61(1-\frac{r}{b})]} \qquad 1 < \frac{r}{b} < 40 \tag{12}$$

$$b = 0.42\left[(\rho_\infty c_p)^{4/5} T_\infty^{3/5} g^{2/5}\right]^{-1/2} \frac{T_m^{1/2} \dot{Q}_c^{2/5}}{\Delta T_m^{3/5}}, \tag{13}$$

where r represents the distance between the fire source and the measuring point in the horizontal direction (m), b represents the characteristic length of the fire plume (m), and $\dot{Q}_c$ is the heat release rate of convection (kW).

Figure 10 plots the longitudinal attenuation of temperature in dimensionless form based on Equation (12). The longitudinal attenuation of temperature in the longitudinal direction of all scenarios collapsed well.

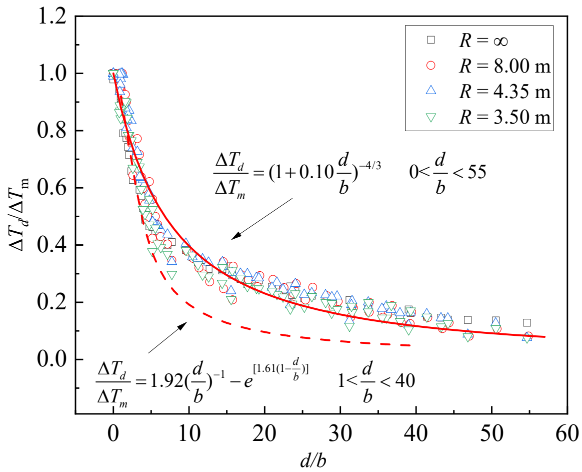

Figure 10. Prediction correlation of longitudinal attenuation of temperature below a ceiling for a scenario with a strong plume-driven ceiling jet.

Equation (12) has also been plotted in Figure 10, where a significant difference can be found between Equation (12) and the experimental data. The reason for such a discrepancy may be attributed to the fact that Equation (12) is proposed for temperature attenuation below an unconfined plate. For fire-induced smoke flow spreading in the tunnel, a region of one-dimensional spreading is formed where the mechanism of smoke spread is distinctly different from that under an unconfined ceiling. According to the fitting results of the experimental data, Equation (14) is more appropriate for predicting the temperature decay in a strong plume-driven tunnel fire. The improved correlation may be more applicable to a large vehicle fire in naturally ventilated tunnels, where the flames can easily impinge on the tunnel ceiling.

A layer of fresh air will be formed that flows to the fire source during tunnel fires under natural ventilation [28]. Studies concerning induced air spread are of interest and will be further studied.

$$\frac{\Delta T_d}{\Delta T_m} = (1 + 0.1\frac{d}{b})^{-4/3} 0 < \frac{r}{b} < 55. \quad (14)$$

4. Conclusions

The distribution characteristics of temperature below a curved tunnel ceiling induced by fire is studied through a small-scale tunnel model. The maximum temperature and longitudinal attenuation of temperature are analyzed. The following are some of the conclusions that may be drawn:

(1) The tunnel turning radius has limited influence on the maximum temperature and the longitudinal attenuation of the temperature below the ceiling in a strong plume impingement scenario. The temperature distribution profiles induced by a strong plume in a curved tunnel have similar tendencies to those observed in a straight tunnel (Figures 4 and 8).

(2) The maximum temperature below the ceiling under strong plume impingement cannot be well-predicted by previously proposed equations based on weak plume assumptions. This is because the thermocouple is in direct contact with the flame and the measured temperature is related to the axial temperature of the fire plume at the ceiling height (Figures 5 and 6).

(3) Improved correlation for predicting the temperature attenuation along the tunnel are proposed based on Heskestad and Hamada's model, which is capable of predicting the temperature decay along the tunnel under a strong plume-driven ceiling jet (Figure 10).

Author Contributions: H.T.: Writing—original draft and funding acquisition. Z.X.: project administration, resources, and supervision. D.Z.: data curation, investigation, validation, and visualization. All authors have read and agreed to the published version of the manuscript.

Funding: This work was supported by the National Key R&D Program of China (Grant No. 2017YFB1201204), the Hunan Provincial Innovation Foundation for Postgraduates (Grant No. CX20190131), and the Fundamental Research Funds for the Central Universities of Central South University (Grant No. 2022zzts0746).

Institutional Review Board Statement: Not applicable.

Informed Consent Statement: Not applicable.

Acknowledgments: We acknowledge the High Performance Computing Center of Central South University for its support.

Conflicts of Interest: The authors declare no conflict of interest.

References

1. Du, T.; Yang, D.; Peng, S.N.; Xiao, Y.M. A method for design of smoke control of urban traffic link tunnel (UTLT) using longitudinal ventilation. *Tunn. Undergr. Space Technol.* **2015**, *48*, 35–42. [CrossRef]
2. Ren, F.; Shi, C.L.; Li, J.; Che, H.L.; Xu, X. Numerical study on the flow characteristics and smoke temperature evolution under double fires condition with a metro train in tunnel. *Tunn. Undergr. Space Technol.* **2021**, *114*, 104553. [CrossRef]
3. Zhang, X.C.; Hu, L.H.; Zhu, W.; Zhang, X.L.; Yang, L.Z. Flame extension length and temperature profile in thermal impinging flow of buoyant round jet upon a horizontal plate. *Appl. Therm. Eng.* **2014**, *73*, 15–22. [CrossRef]

4. Du, T.; Yang, D.; Peng, S.N.; Liu, Y.L.; Xiao, Y.M. Performance evaluation of longitudinal and transverse ventilation for thermal and smoke control in a looped urban traffic link tunnel. *Appl. Therm. Eng.* **2016**, *96*, 490–500. [CrossRef]
5. Tang, F.; He, Q.; Chen, L.F.; Li, P.C. Experimental study on maximum smoke temperature beneath the ceiling induced by carriage fire in a tunnel with ceiling smoke extraction. *Sustain. Cities Soc.* **2019**, *44*, 40–45. [CrossRef]
6. Alpert, R.L. Calculation of response time of ceiling-mounted fire detectors. *Fire Technol.* **1972**, *8*, 181–195. [CrossRef]
7. Heskestad, G.; Delichatsios, M.A. The initial convective flow in fire. *Symp. Int. Combust.* **1979**, *17*, 1113–1123. [CrossRef]
8. Delichatsios, M.A. The flow of fire gases under a beamed ceiling. *Combust. Flame* **1981**, *43*, 1–10. [CrossRef]
9. Li, Y.Z.; Lei, B.; Ingason, H. The maximum temperature of buoyancy-driven smoke flow beneath the ceiling in tunnel fires. *Fire Saf. J.* **2011**, *46*, 204–210. [CrossRef]
10. Hu, L.H.; Huo, R.; Li, Y.Z.; Wang, H.B.; Chow, W.K. Full-scale burning tests on studying smoke temperature and velocity along a corridor. *Tunn. Undergr. Space Technol.* **2005**, *20*, 223–229. [CrossRef]
11. Li, L.M.; Cheng, X.D.; Wang, X.G.; Zhang, H.P. Temperature distribution of fire-induced flow along tunnels under natural ventilation. *J. Fire Sci.* **2012**, *30*, 121–136. [CrossRef]
12. Huang, Y.B.; Li, Y.F.; Dong, B.Y.; Li, J.M.; Liang, Q. Numerical investigation on the maximum ceiling temperature and longitudinal decay in a sealing tunnel fire. *Tunn. Undergr. Space Technol.* **2018**, *72*, 120–130. [CrossRef]
13. Zhang, X.L.; Lin, Y.J.; Shi, C.L.; Zhang, J.P. Numerical simulation on the maximum temperature and smoke back-layering length in a tilted tunnel under natural ventilation. *Tunn. Undergr. Space Technol.* **2021**, *107*, 103661. [CrossRef]
14. Zhang, T.H.; Wang, G.Y.; Hu, H.H.; Huang, Y.D.; Zhu, K.; Wu, K. Study on temperature decay characteristics of fire smoke backflow layer in tunnels with wide-shallow cross-section. *Tunn. Undergr. Space Technol.* **2021**, *112*, 103874. [CrossRef]
15. Tang, F.; Li, L.J.; Chen, W.K.; Tao, C.F.; Zhan, Z. Studies on ceiling maximum thermal smoke temperature and longitudinal decay in a tunnel fire with different transverse gas burner locations. *Appl. Therm. Eng.* **2017**, *110*, 1674–1681. [CrossRef]
16. Tang, F.; Chen, L.; Chen, Y.H.; Pang, H.P. Experimental study on the effect of ceiling mechanical smoke extraction system on transverse temperature decay induced by ceiling jet in the tunnel. *Int. J. Therm. Sci.* **2020**, *152*, 106294. [CrossRef]
17. Ingason, H.; Li, Y.Z. Model scale tunnel fire tests with longitudinal ventilation. *Fire Saf. J.* **2010**, *45*, 371–384. [CrossRef]
18. Chen, L.; Tang, F. Experimental study on the longitudinal temperature decay beneath ceiling in ventilated tunnel fire. *J. Therm. Anal. Calorim.* **2020**, *139*, 3179–3184. [CrossRef]
19. Tao, L.L.; Zeng, Y.H.; Li, J.; Yang, C.C.; Fang, Y.; Li, B.J. Study on the maximum temperature and temperature decay in single-side centralized smoke exhaust tunnel fires. *Int. J. Therm. Sci.* **2022**, *172*, 107277. [CrossRef]
20. Tang, F.; Cao, Z.L.; Chen, Q.; Meng, N.; Wang, Q.; Fan, C.G. Effect of blockage-heat source distance on maximum temperature of buoyancy-induced smoke flow beneath ceiling in a longitudinal ventilated tunnel. *Int. J. Heat Mass Transf.* **2017**, *109*, 683–688. [CrossRef]
21. Zhang, S.G.; Yang, H.; Yao, Y.Z.; Zhu, K.; Zhou, Y.; Cheng, X.D. Numerical Investigation of Back-Layering Length and Critical Velocity in Curved Subway Tunnels with Different Turning Radius. *Fire Technol.* **2017**, *53*, 1465–1793. [CrossRef]
22. Wang, F.; Wang, M.N.; Carvel, R.; Wang, Y. Numerical study on fire smoke movement and control in curved road tunnels. *Tunn. Undergr. Space Technol.* **2017**, *67*, 1–7. [CrossRef]
23. Xu, Z.S.; Zhou, D.M.; Tao, H.W.; Zhang, X.C.; Hu, W.B. Investigation of critical velocity in curved tunnel under the effects of different fire locations and turning radiuses. *Tunn. Undergr. Space Technol.* **2022**, *126*, 104553. [CrossRef]
24. Tang, F.; He, Q.; Sun, X.P.; Jiang, L.; Hu, P.; Hu, L.H. Experimental study of carriage fire in a tunnel: Evolution of flame geometry characteristics under relative strong crosswinds. *Proc. Combust. Inst.* **2021**, *38*, 4963–4970. [CrossRef]
25. Li, Y.S.; Zhang, X.L.; Sun, X.P.; Zhu, N. Maximum temperature of ceiling jet flow in longitudinal ventilated tunnel fires with various distances between fire source and cross-passage. *Tunn. Undergr. Space Technol.* **2021**, *113*, 103953. [CrossRef]
26. Hu, L.H.; Wang, Q.; Tang, F.; Delichatsios, M.A.; Zhang, X.C. Axial temperature profile in vertical buoyant turbulent jet fire in a reduced pressure atmosphere. *Fuel* **2013**, *106*, 779–786. [CrossRef]
27. Heskestad, G.; Hamada, T. Ceiling Jets of Strong Fire Plumes. *Fire Saf. J.* **1993**, *21*, 69–82. [CrossRef]
28. He, L.; Xu, Z.S.; Markert, F.; Zhao, J.M.; Xie, E.; Liu, Q.L.; Fan, C.G. Ceiling jet velocity during the whole process of fire development in a tunnel. *J. Wind Eng. Ind. Aerodyn.* **2021**, *212*, 104588. [CrossRef]